

Chapter

Ferromagnetism in Mn and Fe Doped LuN: A Potential Candidate for Spintronic Application

*Ramesh Sharma, Jisha Annie Abraham,
Jagadish Chandra Mahato, Sajad Ahmed Dar
and Vipul Srivastava*

Abstract

Diluted magnetic semiconductor (DMS) materials have gained a lot of attention in the last decade due to their possible use in spintronics. In this chapter, the effect of transition metal (TM) i.e., Mn and Fe doping on the structural, electronic, magnetic as well as optical properties of pure and doped LuN has been presented from the first principles density functional theory (DFT) calculation with the Perdew-Burke-Ernzerhof-generalized gradient approximation (PBE-GGA) and Tran Blaha modified Becke-Johnson potential (TB-mBJ) as correlation potentials. The predicted Curie temperature is expected to be greater than room temperature in order to better understand the ferromagnetic phase stability, which has also been confirmed through the formation and cohesive energies. The calculated lattice constants for perfect LuN (rock-salt structure) are in good agreement with the experimental values. Interestingly, doping of Mn and Fe on pure LuN displays indirect band gap to a direct band gap with half metallic and metallic character. The detailed analyses combined with density of state calculations support the assignment that the Half-magnetism and magnetism are closely related to the impurity band at the origin of the hybridization of transition states in the Mn-doped LuN. Absorption spectra are blue shifted upon increase in dopant contents and absorption peaks are more pronounced in UV region. The refractive index and dielectric constant show increase in comparison to the pure LuN. According to the Penn's model, the predicted band gaps and static actual dielectric constants vary. These band gaps are in the near visible and ultraviolet ranges, as well as the $\text{Lu}_{0.75}\text{TM}_{0.25}\text{N}$ (TM = Fe, Mn) materials could be considered possible candidates for the production of optoelectronic, photonic, and spintronic devices in the future.

Keywords: density functional theory, spintronics, LuN, doped nitrides, electronic structure, magnetism, optical properties

1. Introduction

Over the past few years, half metallic ferromagnetic materials have gained a lot of interest due to their possible use in spintronic and optoelectronic applications [1, 2]. Every ferromagnetic half-metal consists of two spin versions, one spin is a semiconductor or insulator, while the other is metallic. The rare earth elements,

which have atomic numbers from $Z = 57$ (Lanthanum, La) to $Z = 71$ (Lutetium, Lu), the electronic configuration of these elements is like $[\text{Xe}] 6s^2 4f^n$, where n is zero for La and 14 for Lu [3, 4]. These elements have large orbitals and spin magnetic moments due to their partially filled 4f shells. The rare earth (RE) elements form wide variety of stable nitrides, mononitride and monochalcogenide compounds such as LaN, CeN, EuN, GdN, DyN, HoN, LuN, YN, LuP, LuAs, LuBi, $\text{La}_2\text{Fe}_2\text{S}_5$, HoAgS_2 , GdAgS_2 , YbAgS_2 , etc. Out of these different types of rare earth compounds, rare earth nitrides, attracted immense attention to the condensed matter physicists, material scientists in the last two decades due to their diverse structural, mechanical, magnetic, optical, electronic, and thermal properties [5–18]. The structural properties and structural phase transition at high pressure have been investigated for the rare earth nitrides by a number of groups [7–13]. The thin film of rare earth nitrides can be utilized in spintronic devices and electronic nano-devices [13–16]. The experimental research is being conducted for the realization of rare earth nitrides [7]. Being in the first and last elements of the rare earth series LaN and LuN respectively, theoretical investigation of these two nitrides gives opportunity to probe the closed shell and empty shell 4f electronic properties. Though the effect of rare earth doping in III-Nitrides has been investigated extensively, there are few reports on the investigation of the electronic, magnetic, optical properties available in the literature [19, 20].

In this chapter, we present a detailed theoretical investigation on structure stability, formation energy, electronic band structure, magnetic and optical properties for LuN using a density functional theory (DFT) approach. Most importantly, the effect of Mn and Fe doping on LuN has also been investigated vividly for their optoelectronic applications.

2. Computational method

We have performed the electronic structure calculations in the framework of full potential linearized augmented plane wave (FP-LAPW) method implemented on Wien2k [21] code employed to solve Kohn sham equation based on the density functional theory (DFT) [22, 23]. The treatment of the exchange correlation potential is done within the generalized gradient approximation (GGA) with the Perdew–Burke Ernnerhof scheme [24]. Furthermore, in the process of determining the most accurate electronic band characteristics, especially the band gap E_g , which is compatible with the experiment, modified Becke and Johnson (mBJ) [25] potential is also used. The relativistic effects are taken into account. In the interstitial area, the plane wave sets were used outside the muffin tin sphere and the $R_{\text{MT}}K_{\text{max}} = 7.00$ cutoff value was used but the spherical harmonic expansion was used within the sphere. For the incorporation of the irreducible Brillouin field, 64 k-points mesh was used. The muffin tin radii were chosen, respectively. The separation of the core and valence states in terms of the energy cut-off parameter was adjusted to -6.0 Ry to avoid charge leakage. The 1000 k-points were used for reciprocal space sampling. A series of repeated iterations were used to achieve energy convergence up to 0.01 mRy.

3. Results and discussion

3.1 Structural phase stability

To study the electronic structure and magnetic properties of TM doped LuN, a $1 \times 1 \times 1$ super cell of LuN containing 8 atoms was constructed. **Figure 1a–c** shows

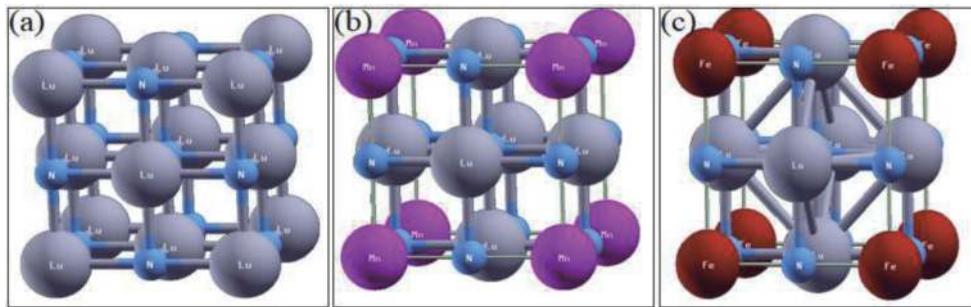


Figure 1. The ball-and-stick model (rock-salt structure) for (a) intrinsic LuN, (b) Mn-doped LuN and (c) Mn-doped LuN unit cell.

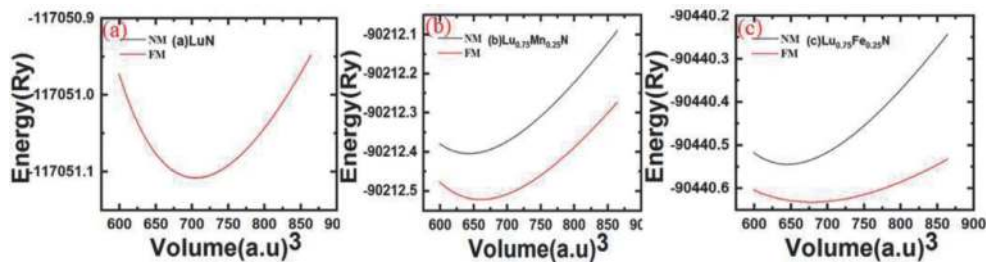


Figure 2. Total energy vs. unit cell volume for the (a) LuN, (b) 25% Mn doped LuN (c) 25% Fe doped LuN. The plot indicates that the 25% Mn and Fe doped LuN possess lower energy in the ferromagnetic phase. The total energy calculations are obtained using PBE-GGA pure and doped LuN.

the ball-and-stick model for the intrinsic LuN, 25% Mn and Fe-doped LuN, respectively. We have considered the rocksalt crystal structure with space group Fm-3 m for the LuN unit cell which is the most stable structure of the bulk LuN. The corner atoms are the lutetium (Lu) atoms surrounded by six nitrogen (N) atoms as shown in **Figure 1a**. In **Figure 1b**, the Mn-doped LuN unit cell has been illustrated. The corner lattice sites have been doped with Mn atoms. In **Figure 1c**, the corner Lu atoms of the rock salt structure have been replaced by Fe atoms for achieving 25% Fe doping of LuN. The equilibrium structure of the pure LuN has been determined by the minimization of total energy vs. unit cell volume using generalized gradient approximation (GGA) method. **Figure 2a–c**, shows the total energy vs. unit cell volume plot for the intrinsic LuN, 25% Mn-doped LuN and 25% Fe-doped LuN, respectively. From the total energy minimization calculation, we have obtained the lattice parameter of the intrinsic LuN as 4.7104 Å. This lattice is very close to the experimentally measured value of 4.766 Å [26]. The calculated lattice parameter is also consistent with the theoretically calculated values by other groups [27, 28]. The equilibrium lattice constant for the 25% Mn-doped LuN in FM phase is calculated to 4.6094 Å and in the NM phase is 4.5674 Å. The equilibrium lattice constant for the 25% Fe-doped LuN in ferromagnetic (FM) phase is calculate to 4.5924 Å and in the non-magnetic (NM) phase is 4.5728 Å. In order to get the equilibrium lattice parameters of the Mn-Fe doped LuN, the total energy vs. unit cell volume size are also calculated by considering the Birch Murnaghan' equation method. The plots for the total energy vs. unit cell volume size are shown in **Figure 2b** and (c), respectively. We found that the value of lattice parameters, and volumes decrease due to incorporation of 3d-TM doping in the pure LuN. It is worth mentioning that both the 25% Mn and Fe-doped LuN are found total energy minimization in two phases i.e. ferromagnetic phase and non-magnetic phase. The values of the optimized lattice parameter, volume, bulk modulus, pressure derivative of bulk modulus

Properties		LuN	Lu _{0.75} Mn _{0.25} N	Lu _{0.75} Fe _{0.25} N
Lattice constant, a (Å)	FM	4.7104	4.6094	4.5924
	NM		4.5674	4.5728
Other theory		4.77 [27] 4.76 [28]		
Experiment		4.76 [26]		
Volume, V (Å ³)	FM	705.2909	660.8789	653.5967
	NM		642.9726	645.2908
Bulk modulus, B (GPa)	FM	186.9883	188.7961	189.2357
	NM		206.7191	202.4745
Pressure derivative of B, B'	FM	4.2116	4.3813	4.2797
	NM		4.4348	4.4452
Total optimized energy (Ry)	FM	-117051.107870	-90212.521303	-90440.631938
	NM		-90212.403516	-90440.544004
T _c (K)		—	747	909
Bond length (Å)		Lu-N = 2.20	Mn-N = 2.3047	Fe-N = 2.296
			N-Lu = 2.3047	N-Lu = 2.296
			Mn-Lu = 3.2593	Fe-Lu = 3.247
Formation energy (eV/atom)		-5.36	-8.540	-8.162
Band gap, E _g (eV)		0.93	Spin up ↑ = 0.43, Spin down = No gap	Spin up ↑ = 1.79, Spin down = No gap
Other theory & exp.		1.173 [27]		
Exp.		1.55,1.6 [26]		
Magnetic Moment (μ _B)		—	Int = 0.08801	Int = -0.09335
			Mn = 4.00700	Fe = 3.94823
			Lu = 2.589	Lu = -0.1032
			N = -0.1209	N = 1.05447
			Tot = 4.00015	Tot = 4.8984
Static dielectric constant ε ₁ (0)		6.40	12.69	19.99
n(0)		2.6	3.2	4.25
R(0)		0.19	0.32	0.423

Table 1.

The ground state properties, bond length (Å), formation energy (eV), band gap (eV), magnetic moment (μ_B) and optical parameters for the pure LuN, and Lu_{0.75}TM_{0.25}N (TM = Fe, Mn).

and total energy of the pure LuN, Mn and Fe doped LuN in nonmagnetic and ferromagnetic phases are presented in **Table 1**.

We have used a relaxed structure in both the FM and NM phases to determine the ground-state energies of Mn and Fe-doped LuN to highlight the actual stable phase. The positive value of E (E = E_{NM} - E_{FM}) indicates that the FM state is more stable (see **Table 1**). The formation energies for LuN, Lu_{0.75}Mn_{0.25}N and Lu_{0.75}Fe_{0.25}N obtained from calculation are to -5.36 eV, -8.540 eV and -8.162 eV, respectively. The negative sign of the formation energy indicates that during creation of the compounds, energy release revealing the stability in the FM state. The cohesive energy (E_{coh}) of Lu_{0.75}TM_{0.25}N (TM = Mn, Fe) compounds are responsible for holding the atoms together in the crystal structure, further confirms the stability of the compounds. The values of E_{coh} are calculated to -2.89Ry, -3.43 Ry and -3.44 Ry for pure and TM-doped LuN (TM = Mn, Fe). The

computed cohesive energies exhibit higher values than their binaries, which again imply FM stability.

After geometry optimization the structure around the TM dopant is slightly suppressed with Lu atoms drawn closer to the TM the relaxed TM-Lu bond length is less than that of the N-Lu bond.

3.2 Electronic properties

The spin polarized band structures of pure LuN, Mn and Fe (25%)-doped LuN are presented in **Figure 3a–f**. An Indirect band gap to direct band gap transition in the band structure of the pure LuN is clearly observed for 25% Mn and Fe substitution at the Lu sites. In the case of pure LuN, the highest occupied state of the electrons occurs at 'T' point, whereas the lowest empty state of the electrons occurs at the 'X' point in the band structure. The indirect band gap of 0.93 eV is obtained from the calculation like that seen experimentally, as shown in **Table 1**. It is to be mentioned here that there is no distinguishable difference observed in the up (\uparrow) spin and down (\downarrow) spin bands as can be seen in **Figure 3a** and **b**. A slight overlap of the spin up (\uparrow) band for the Mn doped LuN whereas total spin down (\downarrow) band exhibits an direct energy gap as can be seen in the **Figure 3c** and **d**. The 25% Mn doped LuN behaves as a half-metallic ferromagnet. In case of Fe doped LuN there is a distinct energy gap in the total spin up (\uparrow) band whereas there is a significant overlapping in the total spin down (\downarrow) band as a result, **Figure 3e** and **f** show that the Fe doped LuN compound is magnetic compound.

The total spin polarized density of states (DOS) and partial density of states (PDOS) obtained using the mBJ-GGA potential, for the pure LuN, Mn and Fe doped LuN as well as spin density of states for the individual atoms in the unit cell are plotted in **Figure 4a–c**. From **Figure 4a**, it is clear that the total spin polarized DOS of the up and down spin states for the Lu atom (red) and N atom (blue) are identical. From the partial spin polarized DOS plots for Lu and N atom, it can be seen that the spin up (\uparrow) band for Lu and N atoms are just symmetric to that of the spin down (\downarrow) band. As a results total (black line) spin polarized spin up (\uparrow) band is symmetric to that of the spin down (\downarrow) band in total for LuN unit cell and the pure LuN exhibits the non-magnetic electronic character with an energy band gap. But from the partial spin density of state plot in **Figure 4b**, it can be seen that the spin down (\downarrow) density of state and spin up (\uparrow) density of state are no more symmetric upon 25% Mn doping in LuN. The spin down (\downarrow) density of state of the Mn atom (green line) in $\text{Lu}_{0.75}\text{Mn}_{0.25}\text{N}$ is completely different in both conduction band and valance band. Due to the delocalized character of the 'd' and 's' electrons in Mn electron density of states appears from nearly 0.1 eV in the conduction band. The peak of the spin down (\downarrow) DOS occurs at 1.2 eV. But there is no contribution to the spin up (\uparrow) density of states of the Mn atom (green line) in $\text{Lu}_{0.75}\text{Mn}_{0.25}\text{N}$ in the conduction band. There is slightly high spin up (\uparrow) DOS compared to that in the spin down (\downarrow) DOS from the Mn atom (green line) in the valance band. Also the contribution is much less compared to that of the Lu atom (red line). The electronic up spin (\uparrow) DOS from the N atom is asymmetric to that of the down spin DOS and it connects the up spin DOS of conduction band to that of the valance band. As a result, there is no gap in the total (black line) up spin DOS of the band structure of the $\text{Lu}_{0.75}\text{Mn}_{0.25}\text{N}$, but there is a gap in the total (black line) spin down DOS of the $\text{Lu}_{0.75}\text{Mn}_{0.25}\text{N}$. Thus $\text{Lu}_{0.75}\text{Mn}_{0.25}\text{N}$ exhibits a half-metallic electronic behaviour. Due to the nature of band filling in minority spin states and majority spin states, $\text{Lu}_{0.75}\text{Fe}_{0.25}\text{N}$ is metallic nature. In metallic $\text{Lu}_{0.75}\text{Fe}_{0.25}\text{N}$, the asymmetry and occupancy of d states of Fe in majority states and p states of N in minority states is evident, led to a significant magnetic moment of Fe.

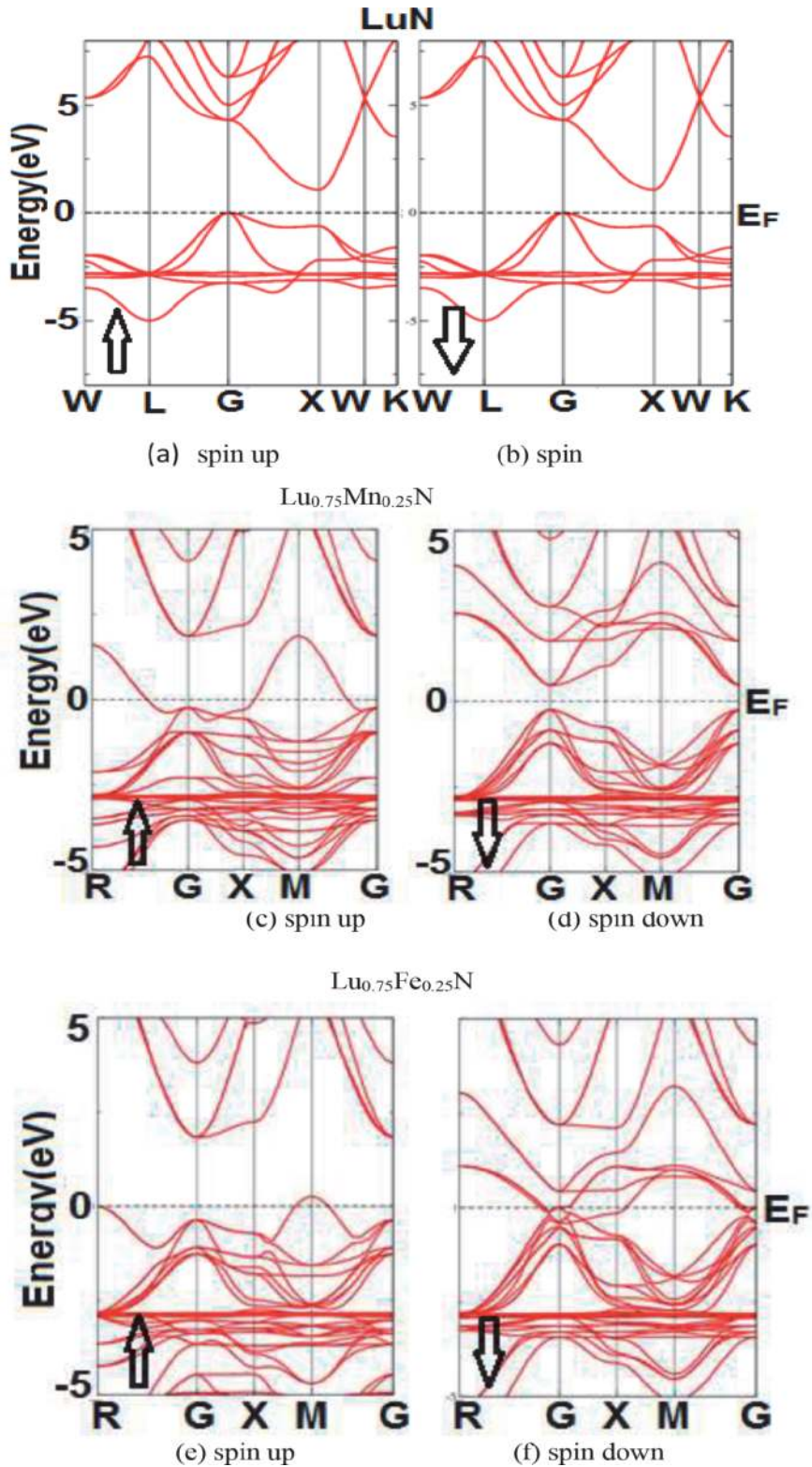


Figure 3. Band structures of $\text{Lu}_{1-x}\text{TM}_x\text{N}$ ($x = 0.25$, $\text{TM} = \text{Mn}, \text{Fe}$) along the high symmetry directions at their equilibrium lattice constants, estimated using mBJ-GGA in figure (a) for $x = 0.0$, (b) for $\text{TM} = \text{Mn}$, $x = 0.25$ and (c) for $\text{TM} = \text{Fe}$, $x = 0.25$.

In Mn-Fe-doped LuN, the interaction arising between 3d-state of Mn/Fe impurities and p-states of host lattice N anions, causes the appearance of the localized states within the band gap at E_F , which induce half-metallic ferromagnetic

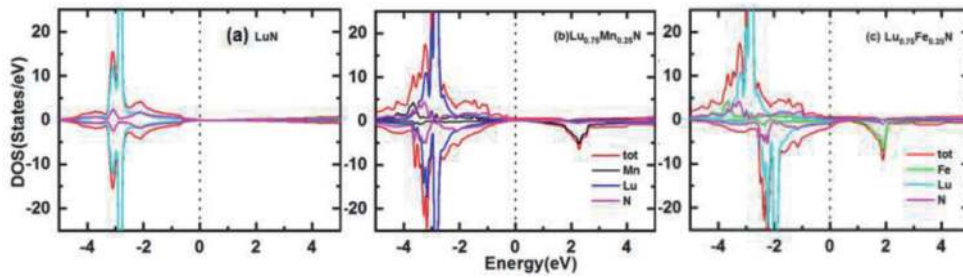


Figure 4. Spin-polarized total and partial DOS for $\text{Lu}_{1-x}\text{TM}_x\text{N}$ ($x=0.25$, $\text{TM}=\text{Mn}$, Fe) obtained using the mBJ-GGA potential (a) for $x=0.0$, (b) for $\text{TM}=\text{Mn}$, $x=0.25$ and (c) for $\text{TM}=\text{Fe}$, $x=0.25$.

characteristics. Therefore, the large splitting of t_{2g} states causes the double exchange mechanism that is responsible for producing ferromagnetism in Mn doped LuN half-metallic semiconductors. The investigated compounds demonstrate a strong p–d exchange interaction within the valence band of LuN, resulting in p-type carrier induced ferromagnetism.

3.3 Magnetic property

The calculated total and partial magnetic moments of individual elements of $\text{Lu}_{0.75}\text{TM}_{0.25}\text{N}$ are reported in **Table 1**. Dopant atoms Mn and Fe are the leading source of the magnetization in $\text{Lu}_{0.75}\text{TM}_{0.25}\text{N}$ ($\text{TM}=\text{Mn}$, Fe) as their magnetic moments are $4.00\mu_B$ and $4.89\mu_B$, respectively. In $\text{Lu}_{0.75}\text{Mn}_{0.25}\text{N}$ compound some N atoms provide negative values of magnetic moment indicating anti-parallel magnetic moment to the Mn and Lu atoms as their magnetic moment values are positive. As the interstitial site holds a positive value of magnetic moment equal to $0.08801\mu_B$, it adds its contribution to the total magnetic moment of the super cell. But in case of $\text{Lu}_{0.75}\text{Fe}_{0.25}\text{N}$ compound interstitial site holds a negative value of magnetic moment which indicates its anti-parallel effect to parallel magnetic moment containing atoms. 3 atoms of Lu contain negative value of magnetic moment which results anti-parallel magnetic moment in the cell. Therefore, it could be said that the atoms that hold negative and positive values of magnetic moment are interacting anti-ferromagnetically. In comparison, there is a difference in total magnetic moments of the two supercells due to the fact that Mn atom has greater magnetic moment value than Fe atom. Also in Mn doped supercell, only N atoms are anti-parallel but in Fe doped super cell Lu atoms, as well as interstitial site magnetic moment values are anti-parallel.

Moreover, Heisenberg model has been employed to estimate the Curie temperature (T_c) of $\text{Lu}_{1-x}\text{TM}_x\text{N}$ compounds by using the expression $T_c = 2\Delta E/3xK_B$ [29], where x represents impurity cation concentration and K_B shows Boltzmann constant. The estimated T_c values for Mn and Fe-doped LuN, as listed in **Table 1**, have been observed to exhibit highest and lowest T_c , respectively. However, all the $\text{Lu}_{0.75}\text{TM}_{0.25}\text{N}$ compounds have shown T_c above room temperature (RT). The decrease in magnetic moment per magnetic ion from $4.00\mu_B$ to $3.94\mu_B$ is caused by changing the dopant from Mn to Fe, which affects the size of the exchange interactions and thus the related T_c . As a result, all of the compounds investigated can be employed in various magnetic devices that operate above room temperature.

Therefore, the studied DMSs are most suitable for spintronic device applications, which also indicate that experimental material properties can efficiently be simulated by employing theoretical methods.

3.4 Optical properties

Motivated by the prospect of using its interesting electronic structure for optoelectronic semiconductor applications, the optical and electronic transport properties of the pure LuN, Lu_{0.75}Mn_{0.25}N and Lu_{0.75}Fe_{0.25}N were calculated. The frequency dependent optical properties were studied and calculated through the dielectric functions. It was realized that the optical properties of a solid can be portrayed by the complex dielectric function $\epsilon(\omega)$, with two parts, real and imaginary as [30].

$$\epsilon(\omega) = \epsilon_1(\omega) + i\epsilon_2(\omega). \quad (1)$$

In this chapter, we focused on the optical parameters such as real part, $\epsilon_1(\omega)$ and imaginary part, $\epsilon_2(\omega)$ of the dielectric functions, refractive indices $n(\omega)$, extinction coefficient $k(\omega)$, absorption coefficient $\alpha(\omega)$, reflectivity $R(\omega)$, optical conductivity $\sigma(\omega)$ and electron energy function $L(\omega)$ of cubic LuN and Lu_{1-x}TM_xN ($x = 0.25$, TM = Mn, Fe) using the mBJ-GGA. **Figure 5a–h** show obtained results from the mBJ-GGA method.

The complex dielectric function $\epsilon(\omega)$ encompasses both intraband and interband transitions. It is observed that intraband attribute mainly in the case of metal or metal

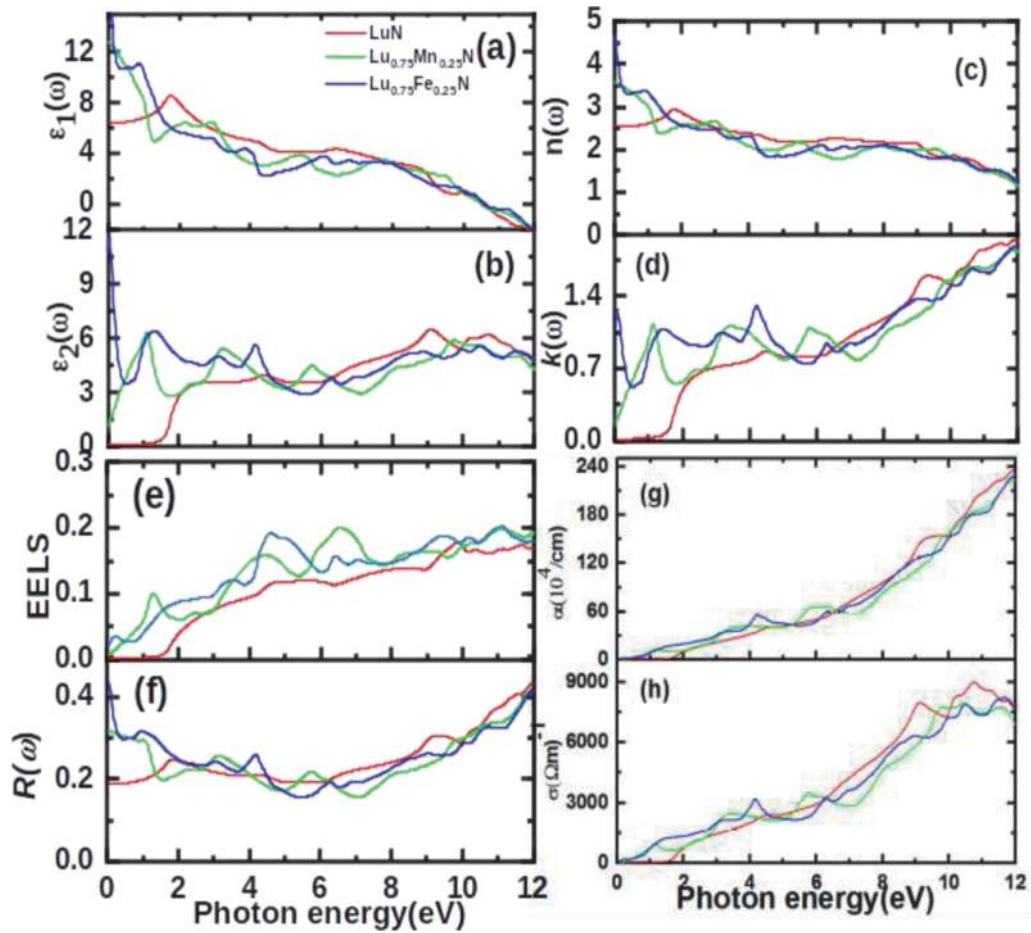


Figure 5. Spectra of the (a) real $\epsilon_1(\omega)$ and (b) imaginary $\epsilon_2(\omega)$ dielectric functions, (c) refractive indices $n(\omega)$, (d) extinction coefficient $k(\omega)$, (e) Absorption coefficient $\alpha(\omega)$, (f) reflectivity $R(\omega)$, (g) optical conductivity $\sigma(\omega)$ and (h) electron energy function $L(\omega)$ of $n(\omega)$ cubic Lu_{1-x}TM_xN ($x = 0.25$, TM = Mn, Fe) obtained using the mBJ-GGA method.

like conductors while in the case of insulating and semiconducting materials, direct as well as indirect transitions contribute to the interband transitions. In this study, we have not treated intraband excitations and indirect interband excitations, which usually contribute very little to $\epsilon(\omega)$. The imaginary part $\epsilon_2(\omega)$ can be obtained from the momentum matrix elements between the occupied and unoccupied wave functions by applying the selection rules, and is computed using the given expression

$$\epsilon_2(\omega) = \frac{e^2 \hbar}{\pi m^2 \omega^2} \sum \int |M_{\nu,c}(k)|^2 \delta[\omega_{\nu c}(k) - \omega] d^3k \quad (2)$$

whereas the real component $\epsilon_1(\omega)$ can be derived from $\epsilon_2(\omega)$ using Kramers-Kronig's relation with the help of following expression [31].

$$\epsilon_1(\omega) = 1 + \frac{2}{\pi} P \int_0^{\infty} \frac{\omega' \epsilon_2(\omega') d\omega'}{(\omega'^2 - \omega^2)} \quad (3)$$

where 'P' represents the principal value of the given integral, 'e' is electronic charge and 'm' is the mass. Since the studied compounds crystallize in cubic phase, one dielectric tensor component is only required for the complete illustration of the optical properties. All other optical constants can be calculated using $\epsilon_1(\omega)$ and $\epsilon_2(\omega)$. We have predicted refractive index $n(\omega)$ from the computed dielectric function, using the following expression:

$$n(\omega) = \left[\frac{\sqrt{\epsilon_1^2(\omega) + \epsilon_2^2(\omega)} + \epsilon_1(\omega)}{2} \right]^{\frac{1}{2}} \quad (4)$$

and, Kramers-Kronig equation has been used to obtain frequency dependent $k(\omega)$ using the following relation

$$k(\omega) = \frac{-2P}{\pi} \int_{\infty}^0 \frac{n(\omega') - 1}{\omega' - \omega} d\omega' \quad (5)$$

Frequency dependent extinction function $k(\omega)$ can also be calculated from $\epsilon_1(\omega)$ and $\epsilon_2(\omega)$ using the expression below,

$$k(\omega) = \left[\frac{\sqrt{\epsilon_1^2(\omega) + \epsilon_2^2(\omega)}}{2} - \frac{\epsilon_1(\omega)}{2} \right]^{\frac{1}{2}} \quad (6)$$

Similarly, the other frequency reliant optical functions such as absorption coefficient $\alpha(\omega)$, optical conductivity $\sigma(\omega)$ and reflectivity $R(\omega)$ can also be computed from the predicted real and imaginary parts of the complex dielectric function.

Using the above expressions these optical parameters are further plotted in **Figure 5**. **Figures 5(a)** and **(b)** represent the variation of real part and imaginary part of the complex dielectric function $\epsilon(\omega)$ in the energy range 0–12 eV in the case of pure LuN and Lu_{1-x}TM_xN (x = 0.25, TM = Mn, Fe). These dielectric plots depict material's capability to allow external electromagnetic field to penetrate through it when 25% concentration of Lu is subjected for doping with Mn and Fe. The dielectric trends depicted by all curves show similar behavior in the entire range except in the static values and in the high energy region, the characteristic distinctions with dielectric maxima at specific energies may correspond to various doping effects. As

seen from **Figure 5(a)**, the static value of real part $\epsilon_1(0)$ is approximately 6.40 for LuN, which drastically increased to 12.69 for Mn-doped LuN and 19.99 for Fe-doped LuN. The real part $\epsilon_1(\omega)$ of pure LuN has a peak at 2 eV, whereas the plots correspond to Mn-doped LuN and Fe-doped LuN show red shift in their dielectric function. After the dielectric maxima, the graph of all three investigated materials starts decreasing gradually and finally falls to zero in the higher energy region. The band gap of the examined materials and the static value $\epsilon_1(0)$ computed from the $n(0)$ by the relation $n(\omega) = \sqrt{\epsilon_1(\omega)}$ spectra are exactly connected according to Penn's model [31]. The plasma frequency and the material band gap are represented by p and E_g , respectively. The imaginary part $\epsilon_2(\omega)$ (see **Figure 5(b)**) of pure LuN has zero value up to 1 eV, after that a rapid rise in its value and increases gradually attaining a peak around 9 eV. While, Mn doped LuN has static value of $\epsilon_2(0)$ as 1.4 and with Fe doping, it sharply rises to 12. The peaks present in the optical spectra of $\epsilon_2(\omega)$ usually occur due to transitions of electrons from the valence to conduction band. The electronic band structures reveal the indirect band gap of 0.93 eV for LuN so the direct optical transitions occur between valence and conduction bands, whereas in the case of Mn doped LuN, it exhibits half-metallic nature, with direct band gap in minority spin channel, but Fe doped LuN shows metallic behavior in both spin channels.

Refractive index $n(\omega)$ is an important optical entity, which shows the response of the light in any type of materials. It is observed that the light depicts different properties upon interaction with different materials, i.e., light may be reflected, refracted, transmitted and diffracted depending on the properties of the materials on which it is incident. Since the velocity of the light varies as it traverses through different materials, hence variations can be observed in the refractive index of the materials for a range of optical spectrum. Overall similar behavior can be observed for refractive index as well as real part of the complex dielectric function $\epsilon(\omega)$ as seen in **Figures 5(a)** and **(c)**. **Figure 5c** represents the optical spectral response of the refractive index of pure LuN and that of $\text{Lu}_{1-x}\text{TM}_x\text{N}$ ($x = 0.25$, TM = Mn, Fe). The high refractive index is presented in the infrared region when light rays traverse through any material. In our present calculations the static refractive index of LuN is 2.5, whereas Mn doped LuN has $n(0)$ as 3.5 and Fe doped LuN has 4.6, respectively, in the low energy region and decreases in high energy region.

It is found from **Figure 5b** and **d** that the optical spectral response of extinction coefficient $k(\omega)$ and imaginary part $\epsilon_2(\omega)$ of dielectric constant illustrate similar profile. It can be seen that $k(\omega)$ also have some threshold energy values similar to imaginary part $\epsilon_2(\omega)$ of the dielectric constant. It is found that the threshold values of incident photon energy for extinction coefficient $k(\omega)$ are approximately 1 eV for cubic LuN and 0 eV for $\text{Lu}_{1-x}\text{TM}_x\text{N}$ ($x = 0.25$, TM = Mn, Fe). The pure cubic LuN shows a smooth increase in the value of extinction coefficient over the studied photon energy range, whereas both doped LuN compounds show several minor peaks in the incident photon range. **Figure 5e**, represents electron energy loss spectroscopy (EELS) function $L(\omega)$ over energy range from 0 to 12 eV, an important parameter depicting the energy loss of fast-moving electron while traversing through the material. The peak associated with the plasma resonance and the corresponding frequency is called plasma frequency. The material exhibits dielectric nature if $\epsilon_1(\omega) > 0$ and metallic nature if $\epsilon_1(\omega) < 0$, above and below plasma frequency. **Figure 5f** represents reflectivity spectra of cubic LuN and $\text{Lu}_{1-x}\text{TM}_x\text{N}$ ($x = 0.25$, TM = Mn, Fe) over an energy range up to 12 eV. The frequency or wavelength dependent reflectivity optical spectrum of the studied pure LuN has a static reflectivity $R(0)$ value as ~ 0.2 up to 1.5 eV, afterwards it shows slight decrease in its value at 6 eV and then gradually

increases in the high energy region. With doping of Fe in LuN, it is observed from **Figure 5f** that static reflectivity $R(0)$ has increased to 0.31 and that of Mn shows that its value rose to 0.45. These results reveal that doping with Fe and Mn has increased the reflectivity of these compounds in the low energy region, which makes them potential candidates of IR reflectors.

Figure 5(g) shows the optical spectral response of the absorption coefficient of LuN and $\text{Lu}_{1-x}\text{TM}_x\text{N}$ ($x = 0.25$, TM = Mn, Fe) over an energy range up to 12 eV. The absorption coefficient provides information about how much incident light energy can be absorbed by the material, when it is exposed to the electromagnetic radiations. All three compounds show similar behavior and it displays the maximum absorption in the high energy region, which indicates that the absorption quality is good for these compounds in ultra violet region of the electromagnetic spectrum, predicting the usage of these materials as good UV absorbers.

When photons are incident on the material, the number of free charge carriers is increased due to absorption of the incident photons, which results in the rise of electrical conductivity, and also results in enhanced photoconductivity. The incident photons should possess adequate energy to excite electrons from the valence band, helping them to cross the band gap and reach the conduction band in the material. **Figure 5(h)** shows the photoconductivity spectrum of the cubic LuN and $\text{Lu}_{1-x}\text{TM}_x\text{N}$ ($x = 0.25$, TM = Mn, Fe). It is seen from **Figure 5(h)** that the photoconductivity of LuN starts 1.8 eV, clearly depicting its semiconducting nature whereas with doping, the photoconductivity starts with zero photon energy due to their metallic nature. The optical conductivity of pure as well as doped compounds increases due to the absorption of photons. The optical conductivity spectra of $\text{Lu}_{1-x}\text{TM}_x\text{N}$ ($x = 0.25$, TM = Mn, Fe) have few maxima and minima peaks in the calculated energy range as also shown in **Figure 5(h)**. The optical spectra studies predicts that the doping of Fe and Mn in LuN makes them potential candidates of UV absorbers as well as IR reflectors, which may be used for fabrication of optical filters in the optoelectronic industry.

4. Conclusions

The structural, electronic, magnetic and optical properties of pure LuN, Mn/Fe doped LuN were investigated under equilibrium conditions by DFT using the PBE-GGA and mBJ-GGA potentials. The positive energy difference between NM and FM states has verified the stability of FM state. The stability of FM state has also been validated by TM-doped DMSs having a lower enthalpy of formation and a higher cohesive energy than the binary un-doped LuN host semiconductor. The Heisenberg classical model, which predicts above-room temperature ferromagnetism, has also predicted the Curie temperature. The calculated electronic properties showed pure LuN to be an indirect band gap semiconductor, and it transforms to a half-metal upon 25% Mn doping, while Fe doping its reveals magnetic nature. The findings presented in this work encourage further experimental research of the electronic structures of RE nitrides. Additionally, the optical characteristics of TM = Mn, Fe-doped LuN DMSs have been predicted in order to investigate future optical applications. The static value of dielectric constants and optical band gaps are observed to vary according to the Penn's model indicating the accuracy of the presented calculations. It has been noted from the imaginary part of the dielectric constant that the studied materials are red-shifted with maximum absorption in the visible as well as in the ultraviolet energy. Therefore, the studied compounds are the best candidates for optoelectronic and spintronic devices.

Acknowledgements

We acknowledge P. Blaha for providing Wien2k code.

Conflict of interest

I confirm there are no conflicts of interest.

Author details

Ramesh Sharma¹, Jisha Annie Abraham², Jagadish Chandra Mahato^{3,4},
Sajad Ahmed Dar⁵ and Vipul Srivastava^{6*}

1 Department of Applied Science, Feroze Gandhi Institute of Engineering and Technology, Raebareli, Uttar Pradesh, India

2 Department of Physics, National Defence Academy, Pune, Maharashtra, India

3 Department of Physics, Ramakrishna Mission Residential College (Autonomous), Kolkata, India


4 Institute of Applied Physics, Technical University Braunschweig, Braunschweig, Germany

5 Department of Physics, Govt. M.A.M College, Jammu, Jammu and Kashmir, India

6 Department of Physics, School of Chemical and Physical Sciences, Lovely Professional University, Phagwara, Punjab, India

*Address all correspondence to: vipsri27@gmail.com

IntechOpen

© 2022 The Author(s). Licensee IntechOpen. This chapter is distributed under the terms of the Creative Commons Attribution License (<http://creativecommons.org/licenses/by/3.0>), which permits unrestricted use, distribution, and reproduction in any medium, provided the original work is properly cited. 

References

- [1] Furdyna JK. Dilute magnetic semiconductors. *J. Appl. Phys.* 1988;**64**:R29. DOI: 10.1063/1.341700
- [2] Ando K. Seeking room temperature ferromagnetic semiconductors. *Science.* 2006;**312**:183. DOI: 10.1126/science.1125461
- [3] Mir SH, Jha PC, Islam MS, Banerjee A, Luo W, Dabhi SD, Jha PK, and Ahuja R. Static and dynamical properties of heavy actinide mononictides of lutetium. *Scientific Reports.* 2016;**6**:29309. DOI: 10.1038/srep29309
- [4] Natali F, Ruck BJ, Plank NOV, Trodhal HJ, Granville S, Meyer S, et al. Rare-earth mononitrides. *Prog. Mater. Sci.* 2013;**58**:1316-1360
- [5] Klemm W, Winkelmann G. To know about the nitrides of the rare earth metals. *Z. Anorg. Allg. Chem.* 1956;**288**:87. DOI: 10.1002/zaac.19562880112
- [6] Larson P, Lambrecht WRL. Electronic structure of rare-earth nitrides using the LSDA+U approach: Importance of allowing 4f orbitals to break the cubic crystal symmetry. *Phys. Rev. B.* 2007;**75**:045114. DOI:10.1103/PhysRevB.75.045114
- [7] Painter GS, Averill FW, Becher PF, Shibata N, Benthem KV, Pennycook SJ. First-principles study of rare earth adsorption at β -Si₃N₄ interfaces. *Phys. Rev. B.* 2008;**78**:21420. DOI:10.1103/PhysRevB.78.214206
- [8] Sreeparvathy PC, Gudelli Vijay Kumar, Kanchana V, Vaitheeswaran G, Svane a, Christensen NE. Thermoelectric properties of binary LnN (Ln = La and Lu). First principles study. *AIP Conf. Proc.* 2015;**1665** (110008). DOI: 10.1063/1.4918064
- [9] Oualdine A, Bentouaf A, Chebli A, Nouamane B, Bouyakoub AZ, Aissa B. Structural, elastic, and electronic properties of CeN and LuN using: Ab initio study. *Journal of Superconductivity and Novel Magnetism.* 2018;**31**:3323-3330. DOI: 10.1007/s10948-018-4604-0
- [10] Singh SK, Verma UP. Investigation of high pressure phase transition and electronic properties of lutetium nitride. *Journal of Physics: Conference Series.* 2015;**640**. DOI: 012029, 10.1088/1742-6596/640/1/012029
- [11] Winiarski MJ, Kowalska D. Electronic structure of REN (RE = Sc, Y, La, and Lu) semiconductors by MBJLDA calculations. *Mater. Res. Express* 2019;**6**:095910. DOI:10.1088/2053-1591/ab31c2
- [12] Vaitheeswaran G, Kanchana V, Rajagopalan M. Structural phase stability and superconductivity of LaN. *Solid State Communications.* 2002;**97-102**(2002):124. DOI: 10.1016/S0038-1098(02)00481-7
- [13] Ludbrook BM, Farrell IL, Kuebel M, Ruck J, Preston ARH, Trodahl HJ, et al. Growth and properties of epitaxial GdN. *J. Appl. Phys.* 2009;**106**:063910-063914. DOI: 10.1063/1.3211290
- [14] Griebel M, Smet JH, Driscoll DC, Kuhl J, Deiz CA, Freytag N, Kadow, Gossard AC, Klitzing KW. Tunable subpicosecond optoelectronic transduction in superlattices of self-assembled ErAs nanoislands. *Nat. Mater.* 2013;**2**:122-126. DOI:10.1038/nmat819
- [15] Jha PK, Sanyal SP. Lattice vibrations in Yb-pnictide compounds. *Phys. Rev. B.* 1995;**52**:15898-15902. DOI: 10.1103/PhysRevB.52.15898
- [16] Larson P, Lambrecht WRL, Chantis A, Van SM. Electronic structure of rare-earth nitrides using the LSDA+U

- approach: Importance of allowing 4f orbitals to break the cubic crystal symmetry. *Phys. Rev. B.* 2007;**7**:1-14. DOI: 10.1103/PhysRevB.75.045114
- [17] Pagare G, Chouhan SS, Soni P, Sanyal SP, Rajagopalan M. First principles study of structural, electronic and elastic properties of lutetium monpnictides. *Comput. Mater. Sci.* 2010;**50**: 538-544. DOI: 10.1016/j.commatsci.2010.09.016
- [18] Legar JM. Chalcogenides and pnictides of cerium and uranium under high pressure. *Physica. B.* 1993;**84-91** (1993):190. DOI: 10.1016/0921-4526(93)90447-E
- [19] O'Donnell K, Dierolf V. Rare earth doped III-nitrides for optoelectronic and spintronic applications. Springer. . DOI: 10.1007/978-90-481-2877-8
- [20] Maity T, Trodahl HJ, Natali F, Ruck BJ, Vézian S. Electron transport in heavily doped GdN. *Phys. Rev. Materials.* 2018;**2**. DOI: 014405, 10.1103/PhysRevMaterials.2.014405
- [21] P. Blaha, K. Schwarz, G.K.H. Madsen, D. Kvasnicka, J. Luitz, WIEN2k, an Augmented Plane Wave plus Local Orbitals Program for Calculating Crystal Properties Vienna University of Technology, Vienna (2001).
- [22] Kohn W, Sham LJ. Self-consistent equations including exchange and correlation effects. *Phys. Rev.* 1965;**140**: A1133. DOI: 10.1103/PhysRev.140.A1133
- [23] Hohenberg P, Kohn W. Inhomogeneous Electron gas. *Phys. Rev.* 1964;**136**:B864. DOI: 10.1103/PhysRev.136.B864
- [24] Perdew JP, Burke K, Ernzerhof M. Generalized gradient approximation made simple. *Phys. Rev. Lett.* 1996;**77**: 3865. DOI: 10.1103/PhysRevLett.77.3865
- [25] Tran F, Blaha P. Accurate band gaps of semiconductors and insulators with a semilocal exchange-correlation potential. *Phys. Rev. Lett.* 2009;**102**: 226401. DOI: 10.1103/PhysRevLett.102.226401
- [26] Duan CG, Sabirianov RF, Mei WN, Dowben PA, Jaswal SS, Tsymbal EY. Electronic, magnetic and transport properties of rare-earth monpnictides: J. *Phys: Condensed. Matter.* 2007;**19**: 315220. DOI: 10.1088/0953-8984/19/31/315220
- [27] Suehiro T, Hirosaki N, Yamamoto Y, Nishimura T, Mitomo M. Preparation of lutetium nitride by direct nitridation. *J. Mater. Res.* 2004;**19**:959. DOI: 10.1557/jmr.2004.19.3.959
- [28] Gupta DC, Bhat IH. Electronic, ductile, phase transition and mechanical properties of Lu-monopnictides under high pressures. *J. Mol. Model.* 2013;**19**: 5343. DOI: 10.1007/s00894-013-2021-7
- [29] Wood DW, Dalton NW. Ferromagnetic curie temperatures of the Heisenberg model with next-nearest-neighbor interactions. *Phys. Rev.* 1967;**159**:384. DOI: 10.1103/PhysRev.159.384
- [30] Ambrosch-Draxl C, Sofo JO. Linear optical properties of solids within the full-potential linearized augmented planewave method. *Comp. Phys. Commun.* 2006;**175**:1-14. DOI: 10.1016/j.cpc.2006.03.005
- [31] Penn D. Wave-number-dependent dielectric function of semiconductors. *Phys. Rev. B.* 1962;**128**:2093. DOI: 10.1103/PhysRev.128.2093